# The Iron Project: RADIATIVE ATOMIC PROCESSES IN ASTROPHYSICS

SULTANA N. NAHAR

*Dept of Astronomy, The Ohio State University, Columbus, OH 43210, USA*
*E-mail: nahar@astronomy.ohio-state.edu*

Astronomical objects, such as, stars, galaxies, blackhole environments, etc are studied through their spectra produced by various atomic processes in their plasmas. The positions, shifts, and strengths of the spectral lines provide information on physical processes with elements in all ionization states, and various diagnostics for temperature, density, distance, etc of these objects. With presence of a radiative source, such as a star, the astrophysical plasma is dominated by radiative atomic processes such as photoionization, electron-ion recombination, bound-bound transitions or photo-excitations and de-excitations. The relevant atomic parameters, such as photoionization cross sections, electron-ion recombination rate coefficients, oscillator strengths, radiative transition rates, rates for dielectronic satellite lines etc are needed to be highly accurate for precise diagnostics of physical conditions as well as accurate modeling, such as, for opacities of astrophysical plasmas.

This report illustrates detailed features of radiative atomic processes obtained from accurate ab initio methods of the latest developments in theoretical quantum mechanical calculations, especially under the international collaborations known as the Iron Project (IP) and the Opacity Project (OP). These projects aim in accurate study of radiative and collsional atomic processes of all astrophysically abundant atoms and ions, from hydrogen to nickel, and calculate stellar opacities and have resulted in a large number of atomic parameters for photoionization and radiative transition probabilities. The unified method, which is an extension of the OP and the IP, is a self-consistent treatment for the total electron-ion recombination and photoionization. It incorporates both the radiative and the dielectronic recombination processes and provides total recombination rates and level-specific recombination rates for hundreds of levels for a wide range of temperature of an ion. The recombination features are demonstrated. Calculations are carried out using the accurate and powerful R-matrix method in the close-coupling approximation. The relativistic fine structure effects are included in the Breit-Pauli approximation. The atomic data and opacities are available on-line from databases at CDS in France and at the Ohio Supercomputer Center in the USA. Some astrophysical applications of the results of the OP and IP from the Ohio State atomic-astrophysics group are also presented. These same studies, however with different elements, can be extended for bio-medical applications for treatments. This will also be explained with some preliminary findings.

*Keywords*: Photoionization; Electron-ion recombination; Oscillator strengths; Di-electronic satellite lines; Opacities

## 1. Introduction

The initial study of an astronomical object can be made via photometry which gives information on location, size, surroundings, etc alongwith low level spectroscopy. Figure 1 shows a photometric image of supernova remnant Cassiopia A[1] composed of infrared data from the Spitzer, visible data from the Hubble Space Telescope, and X-ray data from the Chandra observatory. A supernova remnant typically consists of an outer, shimmering shell of expelled material and a core skeleton of a once-massive star, called a neutron star. Heavy elements in universe are known to be formed during a supernova explosion.

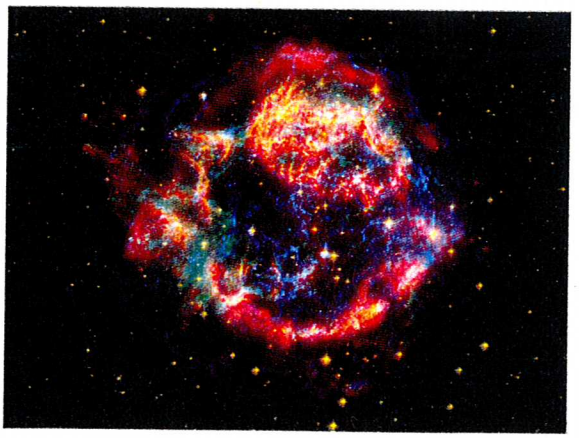

Fig. 1. Photometric picture of Cassiipia A made from observation by Spitzer (infrared), Hubble (visible), and Chandra (X-ray).[1]

However, details such as, temperature, density, speed, composition etc can be obtained only from precise spectroscopy. What we see in an astronomical object depends on how the nuclear energy (gamma rays) produced in the core of the star propagates to the surface. As the radiation travels outward it goes through repeated absorption and emission by atoms and molecules and looses energy to become visible photons. This process depends on the opacity of the constituent materials. Stellar opacities give measures

CP 998, Modern Trends in Physics Research
Third International Conference MTPR-08
edited by L. El Nadi

of radiation transport in the plasmas and are crucial in calculating various quantities and analyzing astrophysical spectra. Opacities depend mainly on oscillator strengths and photoionization cross sections of all transitions in the constituent elements.

About 25 years ago, it was realized that the existing calculated stellar opacities, obtained using atomic data from simple approximations, were incorrect by factors of 2 to 5 resulting in inaccurate stellar models. For example, pulsation periods of Cepheid stars, which are used in gauging the distances of astronomical objects, could not be modeled. A plea was made for accurate opacity using accorate atomic parameters. This initiated the international Opacity Project[2] for precise study of the radiative processes of all astrophysically abundant atoms and ions, from hydrogen to iron, and calculate the opacities. With the same theme, the Iron Project[3] was initiated later for both radiative and collisional process, however, for iron-peak elements and with inclusion of fine structure effect in the calculations. The OP and the IP include a very wide energy range, from infrared (IR), optical (O), ultraviolet (UV), extreme ultraviolet (EUV) to X-rays. The theoretical approach of R-matrix method using close coupling approximation enables consideration of large number of energy levels, and corresponding transitions, and photoionization.

## 2. Radiative Atomic Processes

Astrophysical plasmas are dominated by three radiative atomic processes. (1) Photo-excitation and de-excitation:

$$X^{+Z} + h\nu \rightleftharpoons X^{+Z*}$$

where $X^{+Z}$ is the ion with charge $Z$. The emitted or absorbed photon ($h\nu$) is observed as a spectral line. The relevant atomic parameters for the direct and inverse processes are oscillator strength ($f$) and radiative decay rate ($A$-value).

The other two are the inverse processes of (2) photoionization (PI) and (3) electron-ion recombination. In direct photoionization and radiative recombination (RR), an electron is ejected with absorption of a photon or recombines to a ion with emission of a photon:

$$X^{+Z} + h\nu \rightleftharpoons X^{+Z+1} + \epsilon$$

Photoionization and recombination can also occur via an intermediate state as:

$$e + X^{+Z} \rightleftharpoons (X^{+Z-1})^{**} \rightleftharpoons \begin{cases} e + X^{+Z} & \text{AI} \\ X^{+Z-1} + h\nu & \text{DR} \end{cases}$$

where an electron colliding with a target of charge $+Z$ excites it as well as attaches itself to form a doubly excited quasi-bound state known as an autoionizing state. This state is short-lived and leads either to autoionization (AI) where the electron goes free and target drops to ground state or to dielectronic recombination (DR) where the electron gets bound by emission of a photon. The autoionizing state manifests as an enhancement or resonance in the process. Photoionization resonances can be seen in absorption spectra while recombination resonances can be seen in emission spectra. The relevant atomic parameters for these processes are photoionization cross sections ($\sigma_{PI}$), recombination cross sections ($\sigma_{RC}$) and rate coefficients ($\alpha_{RC}$).

## 3. Theory

The relativistic Hamiltonian of a multi-electron system in Breit-Pauli R-matrix (BPRM) method is given by,

$$H^{\rm BP}_{N+1} = H^{NR}_{N+1} + H^{\rm mass}_{N+1} + H^{\rm Dar}_{N+1} + H^{\rm so}_{N+1}, \quad (1)$$

where the non-relativistic Hamiltonian is,

$$H^{NR}_{N+1} = \left[\sum_{i=1}^{N+1}\left\{-\nabla_i^2 - \frac{2Z}{r_i} + \sum_{j>i}^{N+1}\frac{2}{r_{ij}}\right\}\right] \quad (2)$$

and the three one-body relativisitc terms are mass correction, $H^{mass} = -\frac{\alpha^2}{4}\sum_i p_i^4$, Darwin term, $H^{Dar} = \frac{\alpha^2}{4}\sum_i \nabla^2\left(\frac{Z}{r_i}\right)$, and spin-orbit interation term, $H^{so} = \left[\frac{Ze^2\hbar^2}{2m^2c^2r^3}\right]$ **L.S**. However, the effects of higher order terms, especially the two-body terms, in the Breit-Pauli Hamiltonian,

$$\frac{1}{2}\sum_{i\neq j}^{N}[g_{ij}(so+so') + g_{ij}(ss') + g_{ij}(css') + g_{ij}(d) + g_{ij}(oo')]. \quad (3)$$

where the notation are $c$ for contraction, $d$ for Darwin, $o$ for orbit, $s$ for spin and a prime indicates 'other' can improve the energies and weak transitions. We include full Breit interaction,

$$H^B = \sum_{i>j}[g_{ij}(so+so') + g_{ij}(ss')] \quad (4)$$

for the weak forbidden transitions.

The energies and wavefunctions of the (N+1)-electron system can be obtained from solving

$$H_{N+1}^{BP}\Psi = E\Psi. \tag{5}$$

The close coupling (CC) approximation for wavefunction describe an atomic process as a target or the core ion of N electrons interacting with the (N+1)th electron (e.g. Seaton[4]). Total wavefunction expansion is expressed as:

$$\Psi_E(e+ion) = A\sum_i^N \chi_i(ion)\theta_i + \sum_j c_j\Phi_j(e+ion)$$

where $\chi_i$ is the target ion or core wavefunction at state $i$, $\theta_i$ is the interacting electron wavefunction, which is a continuum state wavefunction $\Psi_F$ when E $\geq 0$ or bound state function $\Psi_B$ when E $< 0$. $\Phi_j$ is a correlation function of (e+ion) compensating the short-range correlation and orthogonality condition. The complex resonant structures in the atomic processes are introduced through couplings of bound and continuum channels in the transition matrix. Substitution of $\Psi_E(e+ion)$ in Hamiltonian equation results in a set of coupled equations which are solved by R-matrix method.

R-matrix method divides the space in two regions, the inner and the outer regions, of a sphere of radius $r_a$ with the ion at the center. $r_a$ is large enough for electron-electon interaction potential to be zero outside the boundary; wavefunction at $r > r_a$ is Coulombic due to perturbation from the long-range multipole potentials. In the inner region, the partial wave function of the interacting electron is expanded in terms of a basis set, called the R-matrix basis.

$$F_i = \sum a_k u_k$$

which satisfies

$$\left[\frac{d^2}{dr^2} - \frac{l(l+1)}{r^2} + V(r) + \epsilon_{lk}\right] u_{lk} + \sum_n \lambda_{nlk} P_{nl}(r) = 0. \tag{6}$$

and are made continuous at the boundary by matching with the Coulomb functions outside the boundary.

For radiative processes, the transition matrix elements $< \Psi_B||\mathbf{D}||\Psi_{B'} >$ for bound-bound transitions and $< \Psi_B||\mathbf{D}||\Psi_F >$ for photoionization and recombination are obtained with dipole operator, $\mathbf{D} = \sum_i \mathbf{r}_i$, where $i$ is the number of electrons. The generalized line strength, $S$, can be obtained as

$$S = \left| \left\langle \Psi_f | \sum_{j=1}^{N+1} r_j | \Psi_i \right\rangle \right|^2 \tag{7}$$

The oscillator strength ($f_{ij}$) and radiative decay rate ($A_{ji}$) for a dipole bound-bound transition are then obtained as

$$f_{ij} = \left[\frac{E_{ji}}{3g_i}\right] S. \;\; A_{ji}(sec^{-1}) = \left[0.8032 \times 10^{10}\frac{E_{ji}^3}{3g_j}\right] S \tag{8}$$

The photoionization cross section, $\sigma_{PI}$, is related to $S$ as

$$\sigma_{PI} = \left[\frac{4\pi}{3c}\frac{1}{g_i}\right]\omega S. \tag{9}$$

where $\omega$ is incident photon energy in Rydberg units and $g_i$ is the statistical weight factor of the initial state.

Recombination cross section, $\sigma_{RC}$, for any level can be obtained from $\sigma_{PI}$ using principle of detailed balance (Milne relation) as

$$\sigma_{RC} = \sigma_{PI}\frac{g_i}{g_j}\frac{h^2\omega^2}{4\pi^2 m^2 c^2 v^2}. \tag{10}$$

These can be summed for the total $\sigma_{RC}$. Recombination rate coefficient in terms of photoelectron energy is given by

$$\alpha_{\mathbf{RC}}(\mathbf{E}) = \mathbf{v}\sigma_{\mathbf{RC}}$$

The recombination rate coefficient, $\alpha_{RC}(T)$, at various temperatures is obtained as

$$\alpha_{RC}(T) = \int_0^\infty v f(v)\sigma_{RC} dv, \tag{11}$$

where $f(v,T) = \frac{4}{\sqrt{\pi}}(\frac{m}{2kT})^{3/2} v^2 e^{-\frac{mv^2}{2kT}}$ is the Maxwellian velocity distribution function. The total $\alpha_{RC}$ is obtained from summed contributions of infinite number of recombined states.

The unified theory for electron-ion recombination considers all infinite recombining levels and subsumes RR and DR in unified manner[5-7] in contrast to existing methods that treat RR and DR separately and the total rate is obtained from $\alpha_{RC} = \alpha_{RR} + \alpha_{DR}$ neglecting the interference between RR and DR. The unified method divides the recombined states in to two groups. The contributions ,from states with $n \leq 10$ (group A) are obtained from $\sigma_{PI}$ using principle of detailed balance, while the contributions from states with $10 < n \leq \infty$

(group B), which are dominated by narrow dense resonances, are obtained from an extension of the DR theory:[6,8]

$$\Omega(DR) = \sum_{J\pi} \sum_{n} (1/2)(2J+1) P_n^{J\pi}(DR). \quad (12)$$

where the DR probability $P_n^{J\pi}$ in entrance channel $n$ is, $P_n^{J\pi}(\mathrm{DR}) = (\mathbf{1} - \boldsymbol{\mathcal{S}}_{ee}^{\dagger}\boldsymbol{\mathcal{S}}_{ee})_n$, $\mathcal{S}_{\mathrm{ee}}$ is the matrix for electron scattering *including* radiation damping. The recombination cross section, $\sigma_{RC}$ in Megabarns (Mb), is related to the collision strength, $\Omega_{\mathrm{RC}}$, as

$$\sigma_{RC}(i \rightarrow j)(Mb) = \frac{\pi \Omega_{RC}(i,j)}{(g_i k_i^2)} (a_o^2/1. \times 10^{-18}), \quad (13)$$

where $k_i^2$ is in Rydberg. The method provides self-consistent set of $\sigma_{PI}$, $\sigma_{RC}$, and $\alpha_{RC}$ as they obtained using the same wavefunction. It also provides level-specific recombination rate coefficients and photoionization cross sections for many bound levels.

Under the IP, $f$, $S$, and $A$-values for fine structure forbidden transitions, and allowed for some complex ions, are treated with relativistic configuration interaction atomic structure calculations using code SUPERSTRUCTURE (SS).[9] The allowed and forbidden transitions are as summarized as: Allowed electric dipole (E1) transtitions are of two types: (i) same-spin multiplet ($\Delta$ j=0,$\pm$1, $\Delta L$ = 0, $\pm$1, $\pm$2, $\Delta$S = 0, parity $\pi$ changes), (ii) intercombination ($\Delta$ j=0,$\pm$1, $\Delta L$ = 0, $\pm$1, $\pm$2, $\Delta$S $\neq$ 0, $\pi$ changes):

$$A_{ji}(sec^{-1}) = 0.8032 \times 10^{10} \frac{E_{ji}^3}{3g_j} S^{E1}, \; f_{ij} = \frac{E_{ji}}{3g_i} S^{\mathrm{E1}}(ij) \quad (14)$$

where $S^{\mathrm{E1}}(ij)$ is the line strength for E1 transition.

Forbidden transitions, which are usually much weaker than the allowed transitions, are of higher order magnetic and electric poles.

i) Electric quadrupole (E2) transitions ($\Delta$ J = 0,$\pm$1,$\pm$2, parity does not change):

$$A_{ji}^{E2} = 2.6733 \times 10^3 \frac{E_{ij}^5}{g_j} S^{E2}(i,j) \ \mathrm{s}^{-1}, \quad (15)$$

ii) Magnetic dipole (M1) transitions ($\Delta$ J = 0,$\pm$1, parity does not change):

$$A_{ji}^{M1} = 3.5644 \times 10^4 \frac{E_{ij}^3}{g_j} S^{M1}(i,j) \ \mathrm{s}^{-1}, \quad (16)$$

iii) Electric octupole (E3) transitions ($\Delta$ J= $\pm$2, $\pm$3, parity changes):

$$A_{ji}^{\mathrm{E3}} = 1.2050 \times 10^{-3} \frac{E_{ij}^7}{g_j} S^{\mathrm{E3}}(i,j) \ \mathrm{s}^{-1}, \quad (17)$$

iv) Magnetic quadrupole (M2) transitions ($\Delta$ J = $\pm$2, parity changes):

$$A_{ji}^{\mathrm{M2}} = 2.3727 \times 10^{-2} \mathrm{s}^{-1} \frac{E_{ij}^5}{g_j} S^{\mathrm{M2}}(i,j). \quad (18)$$

The lifetime of a level can be calculated from the $A$-values, $\tau_k(s) = 1/\sum_i A_{ki}(s^{-1})$

## 4. Results

Results with various features on oscillator strengths and radiative decay rates for bound-bound transitions, photoionization cross sections and recombination rate coefficients are illustrated below.

### 4.1. *Radiative Transitions: f, S, A-values*

Under the IP, E1 transitions are calculated for levels going up to $n$=10 and $l \leq 9$ while weaker forbidden transitions are considered up to $n \leq 5$ in general. The advantage of BPRM method is that a large number of energy levels and transitions can be calculated, however, without spectroscopic identification. Theoretical spectroscopy for level identification, which is a major task, is carried out using quantum defect analysis, percentage of channels contributions, and angular momenta algebra.

For example, a recent BPRM calculations for Fe VX[11] has resulted in 507 fine structure levels and corresponding 27,812 transitions of type E1. The energies are found be within 1% in agreement with the observed values available in NIST[12] compiled table. Table 1 presents an example set of identified energy values grouped together as fine structure compoments of Fe XV.

Close coupling approximation with R-matrix method does not optimize individual transitions. Hence, consistent accuracies are expected in general. Table 2 presents comparison of BPRM transition probabilies of Fe XV[11] with the available values. Good agreement can be seen for most transitions. However, some differences are also exist. Table 2 also presents comparison of A-values for forbidden transitions in Fe XV,[11] obtained from relativistic Breit-Pauli approximation using SUPERSTRUCTURE,[9] with those available in NIST compilation.[12] Good agreement is found between SS and NIST for E2, M1 transitions. Variable agreement is noted between SS and NIST for M2 transitions.

Table 1. Sample set of fine structure energy levels of Fe XV grouped as sets of $LS$ term components. $C_t$ is the core configuration, $\nu$ is the effective quantum number.

| $C_t(S_tL_t\pi_t)$ | $J_t$ | $nl$ | $2J$ | E(Ry) | $\nu$ | $SL\pi$ |
|---|---|---|---|---|---|---|
| Eqv electron/unidentified levels, parity: e | | | | | | |
| 2p63s2 | | | 0 | -3.35050E+01 | 0.00 | 1 S e |
| Nlv(c)= 1 : set complete | | | | | | |
| Nlv= 3, $^3L^o$: P ( 2 1 0 ) | | | | | | |
| 2p63s (2Se) | 1/2 | 3p | 0 | -3.13740E+01 | 2.68 | 3 P o |
| 2p63s (2Se) | 1/2 | 3p | 1 | -3.13214E+01 | 2.68 | 3 P o |
| 2p63s (2Se) | 1/2 | 3p | 2 | -3.11951E+01 | 2.69 | 3 P o |
| Nlv(c)= 3 : set complete | | | | | | |
| Nlv= 1, $^1L^o$: P ( 1 ) | | | | | | |
| 2p63s (2Se) | 1/2 | 3p | 1 | -3.02823E+01 | 2.73 | 1 P o |
| Nlv(c)= 1 : set complete | | | | | | |
| Eqv electron/unidentified levels, parity: e | | | | | | |
| 2p63p2 | | | 0 | -2.84377E+01 | 0.00 | 3 P e |
| 2p63p2 | | | 2 | -2.83981E+01 | 0.00 | 3 P e |
| 2p63p2 | | | 1 | -2.83502E+01 | 0.00 | 3 P e |
| Nlv(c)= 3 : set complete | | | | | | |
| Eqv electron/unidentified levels, parity: e | | | | | | |
| 2p63p2 | | | 2 | -2.81990E+01 | 0.00 | 1 D e |
| Nlv(c)= 1 : set complete | | | | | | |
| Eqv electron/unidentified levels, parity: e | | | | | | |
| 2p63p2 | | | 0 | -2.74705E+01 | 0.00 | 1 S e |
| Nlv(c)= 1 : set complete | | | | | | |
| Nlv= 3, $^3L^e$: D ( 3 2 1 ) | | | | | | |
| 2p63s (2Se) | 1/2 | 3d | 1 | -2.72920E+01 | 2.87 | 3 D e |
| 2p63s (2Se) | 1/2 | 3d | 2 | -2.72822E+01 | 2.88 | 3 D e |
| 2p63s (2Se) | 1/2 | 3d | 3 | -2.72669E+01 | 2.87 | 3 D e |
| Nlv(c)= 3 : set complete | | | | | | |
| Nlv= 1, $^1L^e$: D ( 2 ) | | | | | | |
| 2p63s (2Se) | 1/2 | 3d | 2 | -2.65180E+01 | 2.88 | 1 D e |
| Nlv(c)= 1 : set complete | | | | | | |
| Nlv= 9, $^3L^o$: P ( 2 1 0 ) D ( 3 2 1 ) F ( 4 3 2 ) | | | | | | |
| 2p63p (2Po) | 1/2 | 3d | 2 | -2.50182E+01 | 2.88 | 3 PDF o |
| 2p63p (2Po) | 1/2 | 3d | 3 | -2.49282E+01 | 2.88 | 3 DF o |
| 2p63p (2Po) | 1/2 | 3d | 4 | -2.48254E+01 | 2.86 | 3 F o |
| 2p63p (2Po) | 1/2 | 3d | 1 | -2.45113E+01 | 2.89 | 3 PD o |
| 2p63p (2Po) | 1/2 | 3d | 2 | -2.45045E+01 | 2.88 | 3 PDF o |
| 2p63p (2Po) | 1/2 | 3d | 3 | -2.44046E+01 | 2.88 | 3 DF o |
| 2p63p (2Po) | 1/2 | 3d | 0 | -2.43943E+01 | 2.88 | 3 P o |
| 2p63p (2Po) | 1/2 | 3d | 1 | -2.43941E+01 | 2.89 | 3 PD o |
| 2p63p (2Po) | 1/2 | 3d | 2 | -2.43929E+01 | 2.88 | 3 PDF o |
| Nlv(c)= 9 : set complete | | | | | | |
| Nlv= 3, $^1L^o$: P ( 1 ) D ( 2 ) F ( 3 ) | | | | | | |
| 2p63p (2Po) | 1/2 | 3d | 2 | -2.48346E+01 | 2.88 | 1 D o |
| 2p63p (2Po) | 1/2 | 3d | 3 | -2.37794E+01 | 2.84 | 1 F o |
| 2p63p (2Po) | 3/2 | 3d | 1 | -2.36558E+01 | 2.85 | 1 P o |
| Nlv(c)= 3 : set complete | | | | | | |

Consideration of large number of transitions is needed for opacity calculations, spectral modeling of astrophysical plasmas. Figure 2 shows modeling of Fe I, Fe II, and Fe III lines observed in spectra of active galaxy 1 Zwicky 1. With large number oscillator strengths of Fe I-III in various modelings, agreement is good in general except in shorter wavelength region.

Table 2. Comparison of present $A$-values in unit of $\sec^{-1}$ for E1 transitions with those in NIST[12] compilation from references. The alphabetic letter is NIST accuracy rating.

| $\lambda$ / $\mathring{A}$ | $A$:Ac NIST | $A$(Present) BPRM | SS | $C$ i-j | $SL\pi$ i-j | $g$ i-j |
|---|---|---|---|---|---|---|
| 52.911 | 2.94e+11[1]: C | 2.28e+11 | 2.38e+11 | 3s2 -3s4p | 1S- 1P | 1-3 |
| 59.404 | 3.4e+11[2] : C | 2.40e+11 | 2.23e+11 | 3s3p -3s4d | 1P-1D | 3-5 |
| 307.73 | 4.91e+09[3]:C | 4.78E+09 | 4.91E+09 | 3s3p -3p2 | 3P-3P | 3-3 |
| 65.370 | 3.2e+10[2] : C | 3.70e+10 | 3.52e+10 | 3s3p -3s4s | 3P-3S | 1-3 |
| 65.612 | 9.8e+10[2] : C | 1.14e+11 | 1.06e+11 | 3s3p -3s4s | 3P-3S | 3-3 |
| 66.238 | 1.6e+11[2] : C | 1.95e+11 | 1.82e+11 | 3s3p -3s4s | 3P-3S | 5-3 |
| 224.754 | 1.38e+10[4]:C | 1.35e+10 | 1.40e+10 | 3s3p -3s3d | 3P-3D | 1-3 |
| 227.206 | 1.8e+10[4]:C | 1.76e+10 | 1.83e+10 | 3s3p -3s3d | 3P-3D | 3-5 |
| 227.734 | 9.8e+09[4]:C | 9.68e+09 | 1.0e+10 | 3s3p -3s3d | 3P-3D | 3-3 |
| 69.66 | 1.9e+11[5] : C | 2.18e+11 | 2.16e+11 | 3s3p -3s4s | 1P-1S | 3-1 |
| 243.794 | 4.2e+10[4]:D | 4.09e+10 | 4.25e+10 | 3s3p -3s3d | 1P-1D | 3-5 |
| 63.96 | 1.6e+11[2] : E | 4.61e+10 | 1.97e+11 | 3p2 -3s4f | 1D- 1F | 5-7 |
| 194.067 | 3.8e+08[5]:E | 1.04e+08 | 3.85e+08 | 3p2 -3p3d | 1D-1P | 5-3 |
| 231.68 | 1.5e+10[5]:E | 1.43e+10 | 1.58e+10 | 3p2 -3p3d | 3P- 3P | 3-3 |
| 231.87 | 2.1e+10[5]:E | 2.04e+10 | 2.13e+10 | 3p2 -3p3d | 3P-3P | 3-1 |
| 242.100 | 2.3e+10[5]:D | 6.30e+09 | 2.56e+10 | 3p2 -3p3d | 3P- 3D | 5-7 |
| 68.849 | 9.2e+11[6] : C | 9.15e+11 | 8.66e+11 | 3p3d -3p4f | 3F-3G | 9-11 |
| 69.945 | 7.4e+11[2] :C | 7.25e+11 | 7.29e+11 | 3s3d -3s4f | 3D-3F | 3-5 |
| 69.987 | 7.9e+11[2] :C | 7.67e+11 | 7.72e+11 | 3s3d -3s4f | 3D-3F | 5-7 |
| 70.054 | 8.8e+11[2] :C | 8.63e+11 | 8.70e+11 | 3s3d -3s4f | 3D-3F | 7-9 |
| 70.224 | 4.13e+11[5]:C | 4.23e+11 | 4.12e+11 | 3p3d -3p4f | 3P-3D | 1-3 |
| 73.199 | 8.8e+11[5] :C | 6.89e+11 | 7.95e+11 | 3p3d -3p4f | 1F-1G | 7-9 |
| 73.473 | 6.2e+11[2] :C | 6.01e+11 | 6.12e+11 | 3s3d -3s4f | 1D-1F | 5-7 |
| 312.556 | 1.1e+09[3] :E | 3.51e+09 | 1.01E+09 | 3s3p -3p2 | 3P-1D | 3-5 |
| 238.114 | 3.2e+08[4]:E | 2.85e+08 | 2.81e+08 | 3s3p -3p2 | 3P-1S | 3-1 |
| 191.408 | 3.5e+08[4]:E | 3.53e+08 | 2.67e+08 | 3s3p -3s3d | 3P-1D | 3-5 |
| 196.741 | 1.6e+07[4]:E | 1.45e+07 | 8.49e+06 | 3s3p -3s3d | 3P-1D | 5-5 |
| 304.998 | 3.0e+07[4]: E | 2.20e+07 | 1.17e+07 | 3s3p -3s3d | 1P-3D | 3-5 |
| 305.889 | 2.6e+07[4]: E | 2.63e+07 | 2.34e+07 | 3s3p -3s3d | 1P-3D | 3-3 |
| 38.95 | 1.69e+11[1]: C | 7.4e+10 | 1.56e+11 | 3s2- 3s5p | 1S- 1P | 1-3 |

| $\lambda$ / $\mathring{A}$ | $A$:Ac NIST | $A(sec^{-1})$ SS | $C$ i-j | $SL\pi$ i-j | $g$ i-j |
|---|---|---|---|---|---|
| | | E2,M1,M2 | | | |
| 131.216 | 1.6e+06:D | 1.73e+06 | 2p63s2 -3s3d | 1S-1D | 1-5 E2 |
| 171.913 | 4.3e+04[1]:E | 3.81e+04 | 2p63s2 -3p2 | 1S-3P | 1-5 E2 |
| 178.702 | 4.1e+05[1]:E | 1.59e+05 | 2p63s2 -3p2 | 1S-1D | 1-5 E2 |
| 20080 | 4.4e-01:E | 4.13e-01 | 3p2 -3p2 | 1D-3P | 5-3 M1 |
| 847.43 | 1.90e+02:E | 1.70e+02 | 3s3p -3s3p | 3P-1P | 1-3 M1 |
| 975.84 | 3.0e+01:E | 2.70e+01 | 3p2 -3s3d | 1S- 1D | 1-5 E2 |
| 999.63 | 2.70e+02:E | 2.70e+02 | 3p2 -3p2 | 1D-1S | 5-1 E2 |
| 1019.43 | 1.40e+02:E | 1.24e+02 | 3s3p -3s3p | 3P-1P | 5-3 M1 |
| 1052.00 | 1.400e+03:E | 1.25e+03 | 3p2 -3p2 | 3P- 1S | 3-1 M1 |
| 1283.09 | 2.4e+01 :E | 2.13e+01 | 3p2 -3p2 | 3P- 1S | 5-1 E2 |
| 224.278 | 1.2e+00:D | 31.9 | 3s3p -3s3d | 3P-3D | 1-5 M2 |
| 226.372 | 1.98e+00:C | 26.3 | 3s3p -3s3d | 3P-3D | 3-7 M2 |
| 246.423 | 4.2e+00:D | 40.3 | 3s3p -3p2 | 3P-1S | 2 5-1 M2 |
| 303.494 | 6.4e+00:C | 7.88e+00 | 3s3p -3s3d | 1P-3D | 3-7 M2 |
| 393.980 | 3.39e+00:C | 3.38e+00 | 2p63s2 -3s3p | 1S-3P | 1-5 M2 |

### 4.2. *Photoionization - Cross sections and Resonances*

Similar to oscillator strenghts, IP considers photoionization cross sections $\sigma_{PI}$ for the ground and large number of excited bound states with $n \leq 10$ and $l \leq 9$. CC approximation enables inclusion of extensive resonances in $\sigma_{PI}$ that are not possible with central field approximation. Resonances exist inher-

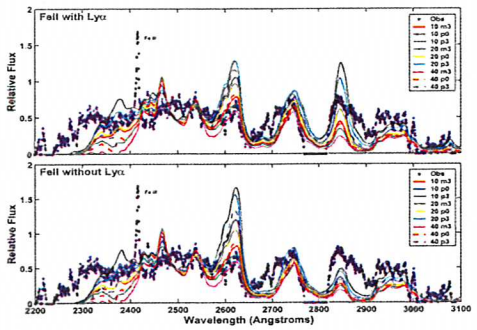


Fig. 2. Modeling of emission spectra of Fe I-III in active galaxy 1 Zwicky 1. Dots - observation; curves - various models with 1000 energy levels, millions of transitions. With (top) and without (bottom) Lyman-alpha fluorescent excitation of Fe II by recombining H-atoms. The models reproduce many of the observed features.

ently in photoionization and recombination processes for all atomic systems with more than one electron. Hence, with no core in hydrogen $\sigma_{PI}$ is smooth, but it shows resonances in two electron helium atom. Fig. 3 presents $\sigma_{PI}$ for the ground states of H[13] and He.[14]

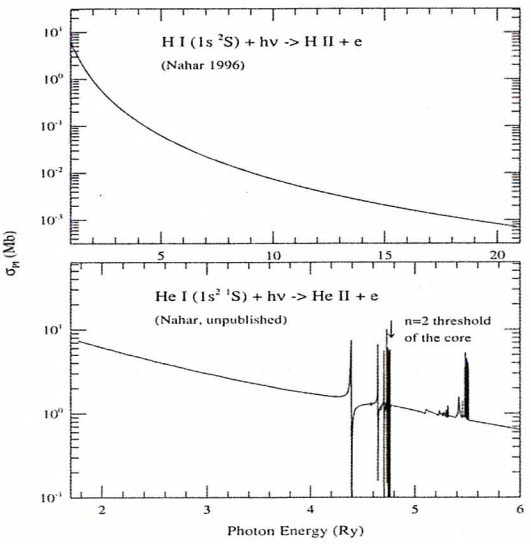


Fig. 3. Photoionization cross sections of ground state of H (top) and He (bottom). While $\sigma_{PI}$ for hydrogen decays smoothly, helium shows resonances due to core excitations. Resonances converge to the excited core threshold; arrow points at n=2 threshold.

Resonant features in photoionization can be of several types. i) The resonances due to Rydberg series of autoinizing states forming at energies $E_p$,

$$(E_t - E_p) = z^2/\nu^2$$

where $E_t$ is an excited core state or threshold and $\nu$ is the effective quantum number of the state. Each excited core state corresponds to a Rydberg series although the resonances may not be prominent for the particular state. These resonances are usually narrow and more common. ii) The resonances due to photoexcitation-of-core, PEC, forming at excited states of the core that are dipole allowed by the core ground state. PEC or Seaton (who interpreted and named them PEC[16]) resonances exist in valence electron excited states only, that is, no PEC resonance for the ground or equivalent electron states, and often are enhanced and wider. iii) Overlapped resonant features forming from Rydberg series of states that belong to closely spaced core levels. iv) Resonances from quasibound equivalent electron states, usually broad, from Coulumb attraction and require atomic structure calculations for their identification. They occur not common. v) Fine structure effects can introduce narrow resonances which are allowed in fine structure, but not allowed in LS coupling.

For a complex system, such as neutral cromium Cr I, the resonant features in photoionization can be intriguing as seen in Fig. 4 which presents $\sigma_{PI}$ of $3d^5 4s(^5P)$ state of Cr I.[15] The entire energy range is filled with extensive narrow resonances. Due to large number of core excitations, 39 in total, in the energy range overlapping of series of resonances is obvious. The background cross section has been enhanced by the first core excited state $3d^5 4s(^6D)$ (pointed by arrow). These structures will provide considerable contributions to quantities such as photoionization rates, recombination rates etc, from low to high temperatures.

The other prominent type of resonance, Seaton or the PEC (photo-excitation-of-core) resonance, forms at an excited core threshold as the core excites to an allowed state while the outer electron remains as a 'spectator' which is followed by photoionization and core dropping to the ground state. It is usually distinguishable because of its wider width and higher peak. A PEC or Seaton resonance is illustrated in Fig. 5 for excited $3d^5\ ^6S4d(^7D)$ state of of Cr I.[15] It exhibits non-hydrogenic nature of an excited state cross sections in contrast to hydrogenic that is often

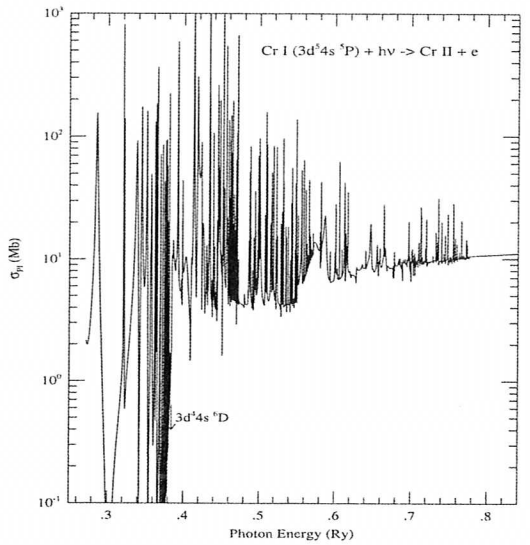


Fig. 4. Photoionization cross sections of $3d^5 4s(^5P)$ state of Cr I[15] showing complex resonant structures due to overlapping of Rydberg series of resonances. The calculation includes excitations of the core to 39 states.

assumed. The enhancement in the background due to a PEC can be orders of magnitude.

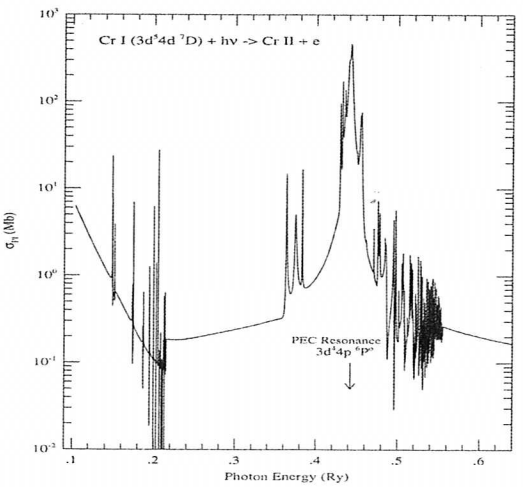


Fig. 5. Illustration of a PEC or Seaton resonance, due to core excitation $3d^5\ ^6S - 3d^4 4p\ 6P^o$ at energy 0.442 Ry (pointed by an arrow), in photoionization cross sections of excited $3d^5\ 6S4d^7D$ state of Cr I.[15] PEC resonance has enhanced the background by orders of magnitude.

### 4.3. *Total and Level-Specific Electron-Ion Recombination*

Electron-ion recombination in low temperature is usually dominated by radiative recombination when the electron combines with an ion by emission of a photon. The electron may not be energetic enough to excite the ion and go through dielectronic recombination. Hence typically the total recombination rate coefficient ($\alpha_R$) starts high at low temperature due to dominance by RR, falls with temperature and then rises again at high temperature due to dominance of DR and forms a DR 'bump' which is followed by monotonic decay at very high temperature. An example showing the typical features of $\alpha_R$ for recombination to a Li-like ion, S XIV,[17] is presented in Fig. 6. The solid curve corresponds to the total unified recombination rate which is being compared with other existing separate RR and DR rates.

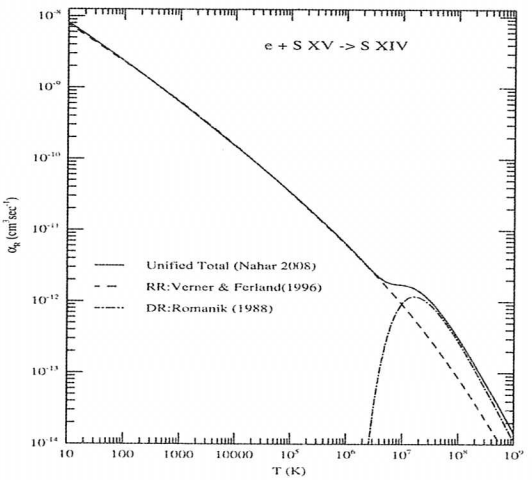


Fig. 6. Total recombination rate coefficients (solid curve) for (e+S XV → S XIV) from unified method that is valid for entire temperature range incorporating both RR and DR.[17] Existing rates are available individually for RR and DR.

The recombination feature often changes for complex atomic systems by forming two or multiple DR 'bump's. The positions of these bumps depend on the resonance positions in photoionzation. For example, one DR bump may form in the low temperature region, such as for recombination of Fe II.[27] In a rare case, almost four bumps may form, as seen in Fig. 7

for recombination to Ar XIII.[19]

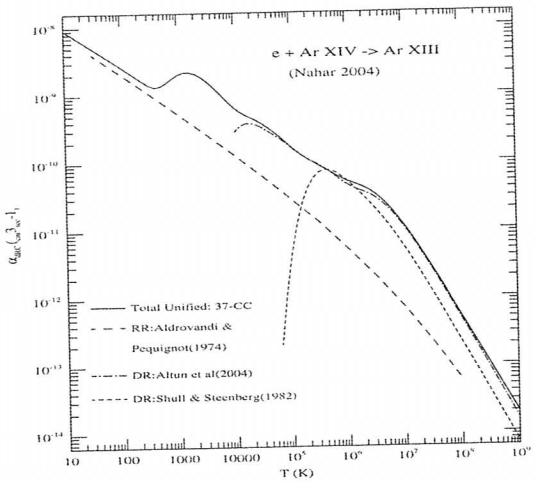


Fig. 7. Unified total recombination rate coefficients of Ar XIII showing multiple DR bumps.[19] Unified rates are compared with available RR and DR rates obtained separately by others.

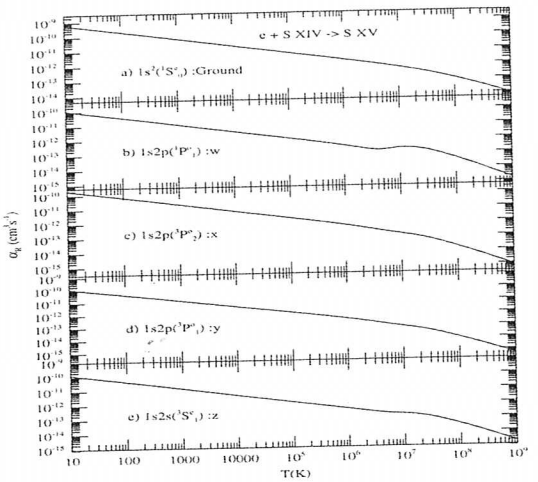


Fig. 8. Level-specific recombination rate coefficients, including RR and DR, of ground and four excited levels, corresponding to four diagpositic w, x, y, z lines, of He-like S XV.[17]

One important advantage of the unified method is to have state-specific recombination rate coefficients $\alpha_R(nLS)$, including both RR and DR, for many bound levels. These are obtained from integration of state-specific photoionization cross sections as explained in the Theory section. Fig. 8 shows level-specific recombination rate coefficients for He-like S XV.[17] The rates correspond to (a) the ground level and four excited levels (b) $2s2p(^1P^o_1)$, (c) $2s2p(^3P^o_2)$, (d) $2s2p(^3P^o_1)$, (e) $2s2s(^3S_1)$ that form the well-known diagnostic allowed $w$, intercombination $y$, and forbidden $x$, $z$ lines of He-like ions for high temperature plasmas. The hydrogenic decay of a level-specific recombination rate changes by a DR bump or shoulder in the high temperature. These rates are needed for the cascade matrix and determination of level populations.

### 4.4. *Unified Method Extension for Dielectronic Satellite Lines*

The unified method for total electron-ion recombination has been extended recently[20] to study the dielectronic satellite (DES) lines. These lines, formed from radiative decay of autoionizing states, are highly sensitive temperature diagnostics of astrophysical and laboratory plasma sources. Most common DES lines in astrophysical spectra are formed by collision of (e+He-like ion) creating a 3-electron Li-like ion. Among DES lines, the 22 DES lines of KLL (1s2l2l') complex below the core excitation $1s^2(^1S_0) \rightarrow 1s2p(^1P^o_1)$ (w-line) are used most because of higher resolution or separation among them, especially for highly charged ions.

The earlier treatment of DES lines is based on isolated resonance approximation (IRA), e.g.,[21] where rate coefficient of a DES line is obtained as,

$$\alpha_R = a_o^3 \frac{g_i}{2g_f} \left[\frac{4\pi}{T}\right] e^{-\frac{\epsilon}{kT}} \frac{A_r A_a}{\sum_m A_a(m) + \sum_n A_r(n)} \tag{19}$$

$\epsilon$ is the DES energy. The single energy point can not provide the natural shape of the DES lines and hence a line profile (or cross section shape depending on one's perspective) is often assumed. IRA treats the resonances essentially as bound features, except for the inclusion of dielectronic capture into, and autoionization out of these levels.

In contrast, the unified method, by including the coupling between the autoionizing and continuum channels, gives the *intrinsic* spectrum of DES lines which includes not only the energies and line strengths as $S = \int_{\epsilon_i}^{\epsilon_f} \sigma_{RC} d\epsilon$ from the unified $\sigma_{RC}$ that includes both RR background and DR, but also

the natural line (or cross section) shapes. Since unified recombination cross sections ($\sigma_{RC}$) include both the resonant and the non-resonant background contributions. the DES spectra correspond directly to resonances in $\sigma_{RC}$. The recombination rate coefficients of DES lines can be calculated from direct integration over the product of the resonant cross sections and temperature-dependent factors.

Using the unified approach, the entire spectra of DES line intensities and recombination rates for the 22 satellite lines of KLL complexes can be produced. Fig. 9 presents the DES spectra of helium-like Fe XXV[20] which is applicable to analysis of K$\alpha$ complexes observed in high-temperature X-ray emission spectra. The top panel (a) presents total spectrum that can be observed and bottom three panels (b-d) present individual component states that contribute to the total spectrum. Individual spectra provides the identification of the DES lines. It may be noted that the natural widths and overlapping of lines are inherently included in the total spectrum. The method was benchmarked by comparing the recombination rates of the DES lines with the existing rates and very good agreement was found for the strong lines.

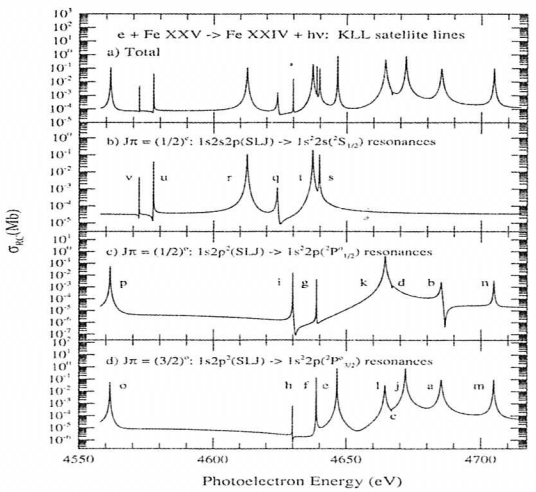


Fig. 9. Satellite lines of Fe XXV in the $K_\alpha$ complex.[20] The top panel (a) shows the total spectrum and the lower three panels show the resolved and identified lines belonging to final recombined level (b) $1s^2 2s(^2S_{1/2})$, (c) $1s^2 2p(^2P^o_{1/2})$, (d) $1s^2 2p(^2P^o_{3/2})$.

## 5. X-ray Spectroscopy from Astronomy to Bio-medical Science

Study of atomic astrophysics research is applicable to medical and nanotechnology research because of similarities. However, interest of atomic species is different from those in astrophysics. We have extended the current investigation to spectral models for X-ray absorption and transmission, and properties of chemical compounds of high-Z elements for possible bio-medical application. Heavy elements, such as gold, interact very efficiently with X-rays with large attenuation coefficients. Ionization and excitation of extended electronic shells have large photoabsorption cross sections up to very high energies. Gold nanoparticles, which are intoxic in living tissues, are being used in study of therapy and diagnostics for cancer treatment. Irradiation with gold nanoparticles in nice cancer has shown reduction of tumor growth.[22] Most of the irradiation methods use broadband radiation that cause sufficient damages. Present work aim in narrow band irradiation using resonant energy ranges.

We have calculated the Auger resonant probabilities and cross sections of gold ions to obtain total mass attenuation coefficients using detailed resonance structures for the K $\longrightarrow$ L,M,N,O,P shell transitions. The X-ray mass absorption is shown in Fig. 10 for gold nanoparticles with vacancies in 2s, 2p subshells. It is seen that X-ray absorption is considerably enhanced by factors of up to 1000 or more at energies of K-shell resonances from K-alpha excitation energy, $\sim$ 67.7 to K-ionization edge at $\sim$82 keV.? This is potentially useful in the calculation of resonant plus non-resonant attenuation coefficients by high-Z elements in plasmas created with high-intensity lasers, monochromatic synchrotron light sources, and electron-beam-ion-traps.

A simulation was carried out for resonant $K_\alpha$ X-ray (68 keV) absorption by gold nanoparticles in tissues. A phantom is assumed where a thin film of Au, 1.0mm/g, is deposited in a tumor 10 cm inside from the skin. As the 68 keV X-rays pass through the phantom, the percentage depth deposition (relative to background) of the radiation due to partial $K\alpha$ attenuation is found to be in complete absorption within $<$ 1 cm of the Au-layer, as shown in Fig. 11. This relates to the development of novel monochromatic or narrow-band X-ray sources.

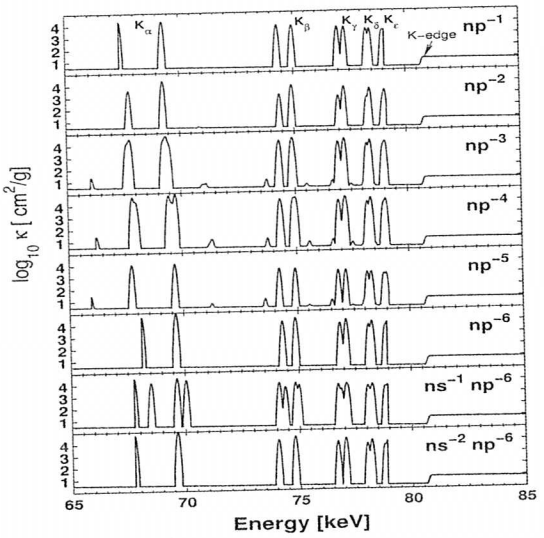


Fig. 10. X-ray mass absorption ($\kappa$) by nano gold particles with 2s, 2p-subshell vacancies via 1s-np K-shell transitions. The K-complexes of resonances, in E = 67.5 - 79 keV, show photo-absorption exceeding the background below the K-edge ionization at 82 keV by large factors.[?]

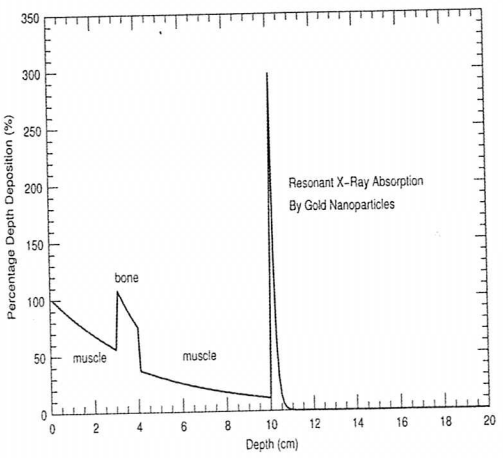


Fig. 11. Percentage depth deposition (relative to background) of 68 keV X-rays irradiated on body tissues where a film of gold nanoparticles of concentration 1.0mm/g is embedded in a tumor 10 cm inside the surface. Deposition due to partial $K\alpha$ attenuation by gold show complete absorption of X-rays within < 1 cm of gold layer.[?]

## 6. Conclusion

Dominant radiative atomic processes, such as photo-excitaions and de-excitations, photoionizatioon, and electron-ion recombination, in astrophyical plasmas are discussed. Features revealed from detailed study of the processes under the Iron Project are reported. Extensions to total and level-specific electron-ion recombination and di-electronic satellite lines provide self-consistent set of atomic data for the inverse processes vio unified theory.

The international collaborations of the Opacity Project and the Iron Project have resulted in large amount of atomic data for the astrophysically abundant atoms and ions from hydrogen to nickel in various ionization stages. They are available through databases, TOPbase and TIPbase at vizier.u-strasbg.fr/topbase/topbase.html and opacities.osc.edu. New and more updated results on photoionization cross sections and recombination cross sections and rates from Ohio State Atomic Astrophysics group (Nahar et al) is available from NORAD webpage at www.astronomy.ohio-state.edu/∼nahar

## Acknowledgments

I would like to thank Professors Fayaz Shahin, Lotfia El-Nadi, and organizers of MTPR08 conference for inviting me for a keynote speech and their kind hospitalities. The research is supported partially by NASA APRA program. The computations were carried out by various Cray computers at the Ohio Supercomputer Center.

## References

1. Imag credit: NASA/JPL-Caltech/STScI/CXC/SAO at http://chandra.harvard.edu/photo/2005/casa/
2. The Opacity Project Team . *The Opacity Project*, Vol 1, 1995, Vol. 2, 1996, Institute of Physics, London UK 1995 and 1996
3. D.G. Hummer *et al.*, *Astron. Astrophys.* **279**, 298 (1993)
4. M. J. Seaton, *J. Phys.* B **20**, 6363 (1987)
5. S.N. Nahar & A.K. Pradhan, *Phys. Rev. Lett.* **68**, 1488 (1992)
6. S.N. Nahar & A.K. Pradhan, *Phys. Rev.* A **49**, 1816 (1994)
7. H.L. Zhang, S.N. Nahar, & A.K. Pradhan, *J. Phys* B **32**, 1459 (1999)
8. R.H. Bell and M.J. Seaton, *J. Phys.* B **18**, 1589 (1985)
9. W. Eissner, M, Jones, H. Nussbaumer, *Comput. Phys. Commun.* 8 **270**, 1974 (

10. spn T,A.A. Sigut, A.K. Pradhan, S.N. Nahar, *Astrophys. J.* **611**, 81 (2004)
11. S.N. Nahar (submitted, 2008)
12. National Institute for Standards and Technology (NIST), compilation atomic data are available at *http : //physics.nist.gov/cgi − bin/AtData/main_asd*
13. S.N. Nahar, *Phys. Rev.* A **53**, 2417 (1996)
14. S.N. Nahar (unpublished)
15. S.N. Nahar (in preparation 2008)
16. Yu Y. & M.J. Seaton, *J. Phys.* B **20**, 6409 (1987)
17. S.N. Nahar, *Open Astron. J.* **I**, 1 (2008)
18. S.N. Nahar, *Phys. Rev.* A **55**, 1980 (1997)
19. S.N. Nahar, *ApJS* **156**, 93 (2004)
20. S.N. Nahar & A.K. Pradhan, *Phys. Rev.* A **73**, 62718-1 (2006)
21. A.H. Gabriel, *MNRAS* **160**, 99 (1972)
22. Hainfeld J *et al. Phys. Med. Biol.* **49**, N309 (2004)
23. A.K. Pradhan *et al* (in preparation 2008)